Journal Name

ARTICLE

Improving the electrochemical performance of $Li_4Ti_5O_{12}$ anode by phosphorus reduction at relatively low temperature

Received 00th January 20xx,
Accepted 00th January 20xx

DOI: 10.1039/x0xx00000x

www.rsc.org/

Wenwen Deng[a]†, Xuyong Feng[b, c]†, Xiang Li[b,c], Sean O'Neill[b,c], Lin Hu[d], Luyao Liu[e], Wai-Yeung Wong[f], Yan-Yan Hu[b,c]* and Chang Ming Li[a, g]*

A novel and efficient method is demonstrated to improve the electrochemical performance of $Li_4Ti_5O_{12}$ and metal-oxide anodes. In contrast to other methods, inexpensive red phosphorus powder is used as a reducing reagent, and the reduction is conducted at a relatively low temperature of 400℃. This method offers a low cost and effective way for $Li_4Ti_5O_{12}$ and metal-oxide anode applications.

Introduction

Lithium-ion batteries have been applied in various portable electronic devices and recently considered as an ideal energy device for electric vehicles.[1] The current commercial Li ion battery comprised of a transitional-metal oxide cathode and graphite anode cannot meet the demands of these vehicles, due to poor rate capability and safety issues (dendritic lithium) of the graphite anode.[2] $Li_4Ti_5O_{12}$ (LTO) is used to replace graphite because it is lithium-dendrite free and exhibits a long cycle life as a result of its minimal lattice expansion (less than 1%) during charge/discharge process.[3] However, the intrinsically poor electronic conductivity has restricted LTO from high rate performance.[4] Many approaches have been carried out to increase the electronic conductivity of LTO,[5-11] which can be categorized into the following three ways: (i) preparation of LTO small-particles with various morphologies; (ii) coating the surface of LTO with carbon or other conductive agents and (iii) Reducing Ti^{4+} to more conductive Ti^{3+}. Among them, reduction of LTO is considered to be the most favorable method for practical applications.[6]

[a] *Institute of Materials Science and Devices, Suzhou University of Science and Technology, Suzhou 215000, P. R. China*
[b] *Department of Chemistry and Biochemistry, Florida State University, Tallahassee, Florida 32306, United States*
[c] *National High Magnetic Field Laboratory, 1800 East Paul Dirac Drive, Tallahassee, FL 32310 (USA)*
[d] *Anhui Province Key Laboratory of Condensed Matter Physics at Extreme Conditions, High Magnetic Field Laboratory of Chinese Academy of Sciences, Hefei 230031, P. R. China*
[e] *College of Chemistry and Molecular Sciences, Wuhan University, Wuhan 430072, China*
[f] *Department of Applied Biology and Chemical Technology, The Hong Kong Polytechnic University, Hung Hom, Hong Kong, P.R. China*
[g] *Institute for Clean Energy & Advanced Materials, Southwest University, Chongqing 400715, P. R. China*
† The authors contribute equally to this work
Corresponding author: Prof. Changming Li, Email: ecmli@swu.edu.cn; Prof. Yan-Yan Hu, Email: hu@ chem. fsu.edu
Electronic Supplementary Information (ESI) available: [Experimental details, SEM, TEM, EDS results and XPS result of ^{31}P, XRD patterns of P, EPR spectrums of LTO, LTO/P samples]. See DOI: 10.1039/x0xx00000x

There are two main ways to reduce Ti^{4+} in LTO to Ti^{3+}. One method is done by using a transition metal, such as Cr, Mo, Cu, Co, or Ta to partially replace Li or Ti in the lattice,[12-18] and another approach is to use reducing reagents.[19] Almost all the reported methods require high temperature (higher than 600℃),[12-19] which limits the application of these approaches.

In this work, we present a novel method to reduce Ti^{4+} in LTO to Ti^{3+} using red phosphorus powder as a reducing reagent, which can sublime at a relatively low temperature (400℃). When LTO and a trace amount of phosphorous powder were mixed and sintered at about 400℃, the red phosphorus was sublimed, taking away O in LTO nanoparticle, forming oxygen vacancies in LTO lattice. X-ray diffraction (XRD), X-ray photoelectron spectroscopy (XPS), and electron paramagnetic resonance (EPR) are employed to examine the change in Ti after phosphorus treatment. Scanning electron microscopy (SEM) reveals that the reduction does not change the morphology of the LTO sample, and high-resolution transmission electron microscopy (HRTEM) shows that the LTO after reduction maintains high crystallinity. The phosphorus treated LTO/P electrode demonstrates greatly improved performance in capacity, rate, and cycling capability when compared to the non-treated LTO electrode. Cyclic voltammetry at different scan rates and EIS results disclose that both Li^+ and electronic diffusion is enhanced for the LTO/P electrode. This simple, inexpensive, and efficient method can also be expanded to improve the electrochemical performance of other metal-oxide anode materials such as MoO_3.

Results and discussions

LTO was synthesized via solid-state reaction at 800℃.[4] 1 wt % red phosphorus powder was used as the reduction reagent to modify LTO and the oxidation product of red phosphorus (P_2O_5) sublimes at 360°C. The non-modified LTO was a white powder (Figure 1a, inset) and the red phosphorus grinded LTO sample (LTO+P) was pink colored (Figure 1a, inset), while the color of LTO/P sample turned to blue (Figure 1a, inset), which is a typical signal for the appearance of Ti^{3+}

and oxygen vacancies in LTO.[12,20] Fig. 1(a) shows the XRD patterns of LTO, LTO+P and LTO/P samples. It can be observed that all XRD peaks for these three samples are sharp, which implies high crystallinity. Moreover, all these diffraction peaks are well indexed to a cubic spinel structure of $Li_4Ti_5O_{12}$ (space group: **Fd-3m**, JDPDS, No. 49-0207). No diffraction peaks for red phosphorous (Figure S1) can be found from LTO+P, since red phosphorous is amorphous and the amount is low. However, when zooming in on the peak that is attributed to 111 planes, we can observe that the diffraction angle (2θ) increases slightly for the LTO/P sample (18.34° for pristine LTO and LTO+P, 18.45° for LTO/P). On the basis of Bragg's equation, the higher diffraction angle means a smaller lattice parameter, which is probably due to the reduction of Ti^{4+} to Ti^{3+} and generated oxygen vacancies.[6]

To confirm the existence of Ti^{3+}, XPS and EPR characterization were performed. The XPS results of the Ti 2p spectra for pristine LTO and LTO/P samples were compared in Figure S2. As can be seen, two new peaks at 463.1 and 457.3 eV which are characteristic peaks of Ti^{3+} appeared in the LTO/P sample, suggesting the potential reduction of Ti^{4+} to Ti^{3+}. The EPR measurement was conducted at 140 K in order to further prove the existence of Ti^{3+}. As can be seen in Figure 1b, a peak at 332 MHz is shown for the LTO/P sample, according to Shiraishi et al.,[21] it can be ascribed to Ti^{3+} ($g = 0.07145 \times \gamma$ (MHz)/H (mT) =1.98), again confirming the potential reduction of Ti^{4+} to Ti^{3+} in the LTO lattice after phosphorus treatment. Furthermore, we examined the EPR spectrum for LTO/P sample at room temperature to see whether there are signals for oxygen vacancies. As can be seen in Figure S3, three signals appear at g=2.038, 2,008, and 1.975, which should be attributed to single electron trapped in the oxygen vacancies according to the reference.[22]

The morphology of the LTO powder before and after phosphorus treatment was characterized by SEM and TEM. The SEM image in Figure S4 shows that LTO possesses submicron sized particles connected to form a percolated network, and high magnification SEM image shows that the surface of LTO is rough (Figure S2b). For the LTO/P particles, the morphology is extremely similar to that of LTO, indicating that the phosphorus reduction did not disturb the basic morphology of LTO. The TEM images show that the LTO and LTO/P nanoparticles have particle sizes ranging from 30 to 100 nm (Figures S5a and S5d). HRTEM images (Figures S5b-c and S5e-f) reveal that both LTO and LTO/P samples are highly crystalline with a spinel structure. The energy dispersive X-ray spectroscopy (EDS) mapping analysis (Figure S6) shows that the LTO/P sample contains about 0.48 wt% phosphorus, which is less than that from LTO+P and means partly P gets evaporated in the form of P_2O_5. XPS was used to analyze the oxidation state of P_{2p} in the LTO/P sample. As was shown in Figure S7, the peak located at ~133 eV is assigned to metal phosphate, which is most probably Li_3PO_4, implying that the red phosphorus was oxidized from 0 to +5 valences and reacted with excess Li from the pristine LTO. Since only 1 wt% red phosphorus powder was used, the amount of Li_3PO_4 formed on the surface of LTO/P is negligible. Li_3PO_4 is ionically conductive which might help improve the ion diffusion between electrolyte and electrode, and thus improve the electrochemical performance.

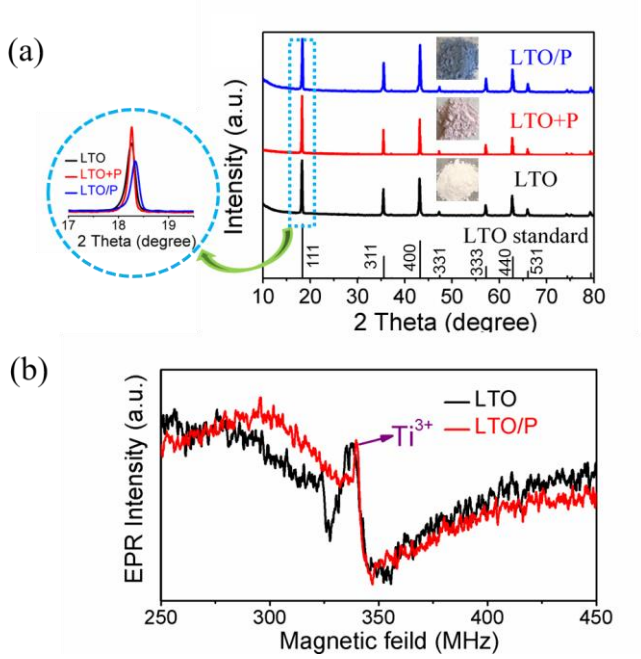

Figure 1 (a) XRD patterns of LTO, LTO+P, LTO/P samples, (b) Electron spin resonance spectra of LTO and LTO/P samples conducted at 140K.

Figure 2 shows the electrochemical performance of the LTO and LTO/P electrodes. As can be seen from Figure 2a-b, when cycled at 0.2 C (1 C= 170 mA g^{-1}), LTO and LTO/P electrodes delivered a capacity of 165 and 170 mAh g^{-1}, respectively. Meanwhile, the LTO/P electrode showed less hysteresis (ΔV, Figure 2b) than LTO electrode (Figure 2a). With the increase of current density, the overpotential of the LTO electrode increased dramatically, while that of the LTO/P electrode increased slowly, indicating smaller polarization for the LTO/P electrode during charging/discharging. It is observed that two discharge plateaus appear at 16 C in Figure 2b, which is attributed to different Li insertion processes. Normally, Li^+ from site 8a would transfer to 16c site during discharging, however, at high discharge rate, this transfer might not happen, leading a different plateau. We discussed this phenomenon in our previous works.[4,9] Furthermore, as can be seen from Figure 2c, when the rate increased to 4 C, the capacity of LTO electrode decreased rapidly to 100 mAh g^{-1}, while the LTO/P electrode can still maintain a capacity of 140 mAh g^{-1}. Even at a rate of 16 C, the LTO/P electrode can still deliver a capacity of 75 mAh g^{-1}, which is very promising for high-rate applications of LTO. Moreover, the LTO/P electrode demonstrate a much better cycling stability than the pristine LTO electrode. As can be seen in Figure 2d, after cycled at 1 C for 160 times, the LTO electrode maintained a capacity of 140 mAh g^{-1}, while the LTO/P electrode can maintain a capacity of 156 mAh g^{-1}, corresponding to a capacity retention of 96%, which is advantageous compared with the capacity retention of the pristine LTO electrode (90%). The superior electrochemical performance for LTO/P electrode should be attributed to oxygen vacancies and Ti^{3+} created by phosphorus reduction, because it has been reported that oxygen vacancies and Ti^{3+} could enhance the electrical conductivity and lithium storage properties of the LTO electrode. [20,23,24]

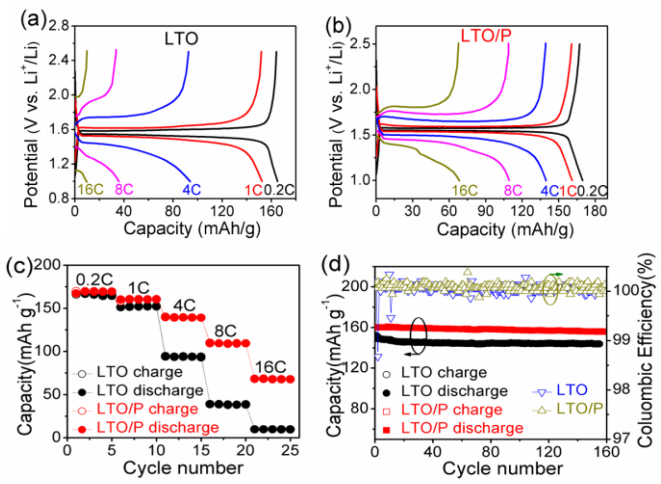

Figure 2 Charging/discharging profiles at different rates for LTO (a) and LTO/P (b) electrodes; (c) cycling stability of LTO and LTO/P electrodes at different rates; (d) cycling stability of LTO and LTO/P electrodes at 1 C.

To better understand the reason why phosphorus reduction enhanced the electrochemical performance of LTO, we conducted CV and EIS analysis. Figure 3a-b is the CV test for LTO and LTO/P electrodes at different scan rates (from 0.2 to 0.8 mV s^{-1}). As can be observed, the CV profiles for LTO and LTO/P electrodes are similar. To clearly illustrate the difference, the peak current i_p (mA) for cathodic and anodic scan is plotted against the square root of the scanning rate ($(V/s)^{1/2}$) as presented in Figure 3c-d. For Faradaic processes, i_p and $v^{1/2}$ are linearly correlated.[4]

$$i_p = (2.69\times10^5)\, n^{3/2} A D_{Li+}^{1/2} C_{Li+} v^{1/2} \quad (1)$$

where n is the number of electrons involved on each charge carrier (n=1 for Li^+), A (cm^2) is the surface area of the electrode, C_{Li+}(moles/cm^3) is the bulk concentration of Li^+ (0.03) and D_{Li+}(cm^2/s) is Li^+ diffusivity. According to equation (1), the calculated D_{Li+}s for LTO and LTO/P electrodes at cathodic scan are 3.69×10^{-13} and 4.73×10^{-13} cm^2/s, respectively. While at anodic scan, the D_{Li+}s for these two electrodes are 2.84×10^{-13} and 3.68×10^{-13} cm^2/s, respectively. This suggests that during charging and discharging the LTO/P electrode demonstrates a slightly higher D_{Li+} than the LTO electrode. EIS was measured for the LTO and LTO/P electrodes. The AC impedance spectrums are fitted with two different equivalent circuits as shown in the inset in Fig. 3e-f. After the 1st cycle, an obvious semicircle can be seen for both LTO and LTO/P electrodes. An intercept at the Z' real axis in the high frequency represents the resistance of the electrolytes (R_s), while the semicircles ending at the frequency of 40 Hz and 158 Hz, respectively, are characteristics of charge transfer resistance (R_{ct}). After the 20th cycle, two semicircles appear for both samples, in which the semicircle in the high frequency region corresponding to R_1 is characteristic of the surface film formed on the electrodes,[25] while the semicircle in the low frequency region is characteristic of the charge transfer resistance (R_{ct}) related to the lithium ion interfacial charge transfer. The relatively high R_{ct} for both samples at the beginning (1st cycle) is due to the bad wetting between electrolyte and electrode. Further, Figure 3e shows that LTO/P has lower R_s than LTO, indicating that the former has better wettability than the latter and it can be ascribed the existence of Ti^{3+} in the former improved the conductivity. After 20 cycles, the resistance for both samples decreases to less than 100 ohms, which may due to the wetting of electrodes after cycling that promoted the Li^+ diffusion. After 20 cycles, the wettability for both electrodes become better, so the R_s decreased and got close. It can be noticed in Figure 3f that the R_{ct} for LTO/P (10 Ω) is about 1/5 of LTO electrode (50 Ω), indicating a sharply decreased interfacial resistance for fast charge transfer process of the phosphorus treated sample during charging/discharging due to more Ti^{3+} in LTO/P sample.[6,13] Therefor, it can be concluded that more Ti^{3+} in LTO/P is not only beneficial for the charge transfer process, but also can reduce R_s. What's more, the overall electrode resistance (R_1+R_{ct}) for LTO/P (15 Ω) is 3 times less than that of LTO electrode (60 Ω) resulting in better rate performance.

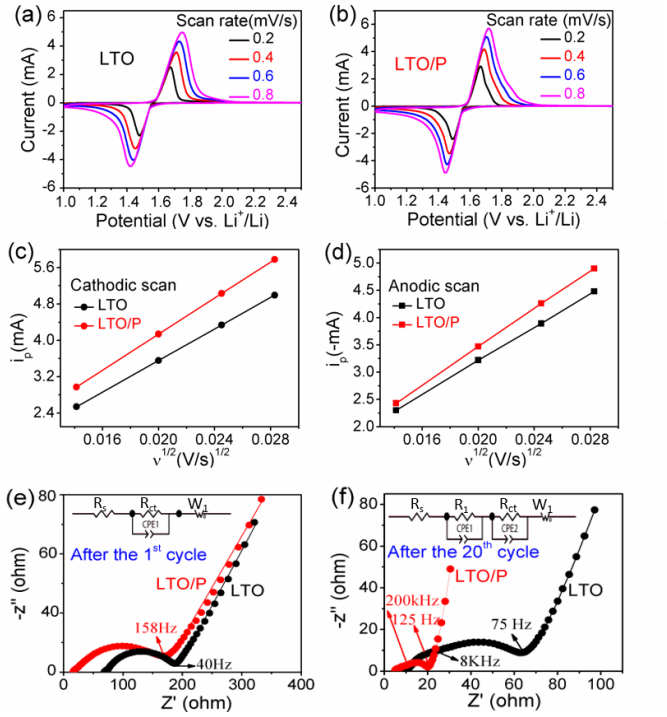

Figure 3 Cyclic voltammetry of half-cell batteries employing (a) LTO and (b) LTO/P electrodes; a plot of the peak current i_p vs. the square root of voltage scanning rate for LTO and LTO/P electrodes at (c) cathodic and (d) anodic scan; The fitted Nyquist plots of LTO and LTO/P electrodes (e) after the 1st cycle and (f) after 20 cycles, frequency range: 0.1 Hz to 5×10^6 Hz.

Phosphorus reduction was also conducted on MoO_3 to partially reduce Mo^{6+} and test its effect on the metal oxide electrode. MoO_3 was mixed with 1 wt% red phosphorus powder and sintered in vacuum at 400 ℃ for 2 h. Electrochemical performance of MoO_3 and phosphorus treated MoO_3 electrode (marked as MoO_3/P) is shown in Figure 4. As can be seen, the MoO_3/P electrode delivers a capacity of 250 mAh g^{-1}, MoO_3 electrode delivers a capacity of 280 mAh g^{-1} at first cycle. However, MoO_3/P electrode shows better rate performance (Figure 4b), with a rate of 10 C, the MoO_3/P electrode can deliver a capacity of 40 mAh g^{-1}. The improved rate capability of MoO_3/P electrode may due to the oxygen vacancies that is brought about by phosphorus reduction.

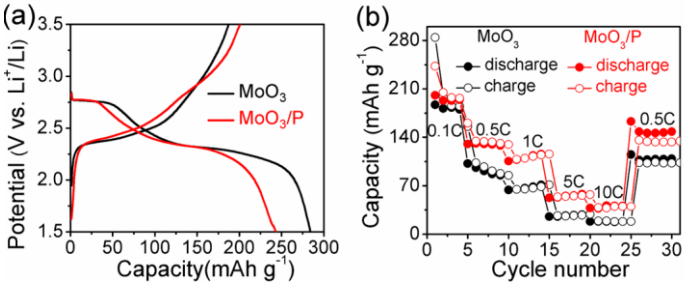

Figure 4 a) Charging/discharging profiles for MoO_3 and MoO_3/P electrodes at 0.1 C (1 C= 300 mAh g^{-1}); b) cycling of MoO_3 and MoO_3/P electrodes at different rates.

Conclusions

In brief, a novel, simple and efficient method is introduced to reduce the transitional metal Ti^{4+} to the more conductive Ti^{3+} and induce oxygen vacancies in $Li_4Ti_5O_{12}$ lattice. Red phosphorus powder is used as a reducing agent due to its sublimation at a relatively low-temperature of 400 ℃. XPS, XRD, and EPR characterization results prove the existence of Ti^{3+}. Electrochemical performance reveals that the phosphorus treatment improves the capacity, rate, and cycling capability of the LTO electrode. Cyclic voltammetry at different scan rates and EIS results disclose that both Li^+ and electronic diffusion is enhanced for the LTO/P electrode. Extended experiments on MoO_3 also show a positive result, indicating that phosphorus reduction can be effective for other metal oxide electrode materials. This method requires a relatively lower temperature than the reported similar works, which could greatly save on production costs and is favorable for the practical applications of the LTO material and even universal uses for other metal oxide electrode materials.

Conflicts of interest

There are no conflicts to declare.

Acknowledgements

This work was supported by The Natural Science Foundation of the Jiangsu Higher Education Institution of China (Grant No. 18KJB150029), the Natural Science Foundation of Jiangsu Province (N0. SBK2018042005), the Research Start-up Foundation (No. 331812150) and Natural Science Foundation (No. XKZ2017006) of Suzhou University of Science and Technology. We also thank the support from National Science Foundation of United States (Grant No. DMR-1808517). W.-Y.W. acknowledges the financial support from the Hong Kong Research Grants Council (PolyU 153051/17P), Hong Kong Polytechnic University (1-ZE1C), and Ms Clarea Au for the Endowed Professorship in Energy (847S).

References

1 N. Nitta, F. Wu, J. T. Lee and G. Yushin, *Mater. Today*, 2015, **18**, 252–264.
2 I. Belharouak, G. M. Koenig and K. Amine, *J. Power Sources*, 2011, **196**, 10344–10350.
3 T. F. Yi, L. J. Jiang, J. Shu, C. B. Yue, R. S. Zhu and H. B. Qiao, *J. Phys. Chem. Solids*, 2010, **71**, 1236–1242.
4 X.Y. Feng, X. Li, M. Tang, A. Gan and Y.-Y. Hu, *J. Power Sources*, 2017, **354**, 172–178.
5 H.G. Jung, J. Kim, B. Scrosati and Y. K. Sun, *J. Power Sources*, 2011, **196**, 7763–7766.
6 H. Zou, X. Liang, X. Feng and H. Xiang, *ACS Appl. Mater. Interfaces*, 2016, **8**, 21407–21416.
7 D. Capsoni, M. Bini, V. Massarotti, P. Mustarelli, S. Ferrari, G. Chiodelli, M. C. Mozzati and P. Galinetto, *J. Phys. Chem. C*, 2009, **113**, 19664–19671.
8 X. Zhang, H. Tian, X. Wang, G. Xue, Z. Tian, J. Zhang, S. Yuan, T. Yu and Z. Zou, *Mater. Lett.*, 2013, **100**, 51–53.
9 X. Feng, H. Zou, H. Xiang, X. Guo, T. Zhou, Y. Wu, W. Xu, P. Yan, C. Wang, J.-G. Zhang and Y. Yu, *ACS Appl. Mater. Interfaces*, 2016, **8**, 16718–16726.
10 X. Feng, C. Shen, N. Ding and C. Chen, *J. Mater. Chem*., 2012, **22**, 20861–20865.
11 X. Feng, N. Ding, Y. Dong, C. Chen and Z. Liu, *J. Mater. Chem. A*, 2013, **1**, 15310–15315.
12 Q. Zhang, C. Zhang, B. Li, D. Jiang, S. Kang, X. Li and Y. Wang, *Electrochim. Acta*, 2013, **107**, 139–146.
13 Q. Zhang, C. Zhang, B. Li, S. Kang, X. Li and Y. Wang, *Electrochim. Acta*, 2013, **98**, 146–152.
14 T.F. Yi, Y. Xie, L. J. Jiang, J. Shu, C. B. Yue, A. N. Zhou and M. F. Ye, *RSC Adv.*, 2012, **2**, 3541.
15 S. Huang, Z. Wen, X. Zhu and Z. Gu, *Electrochem. Commun.*, 2004, **6**, 1093–1097.
16 C. Lin, M. O. Lai, L. Lu, H. Zhou and Y. Xin, *J. Power Sources*, 2013, **244**, 272-279.
17 W. Wang, H. Wang, S. Wang, Y. Hu, Q. Tian and S. Jiao, *J. Power Sources*, 2013, **228**, 244-249.
18 C. Zhang, D. Shao, J. Yu, L. Zhang, X. Huang, D. Xu and X. Yu, *J. Electroanal. Chem.,* 2016, **776**, 188–192.
19 M. R. Jo, K. M. Nam, Y. Lee, K. Song, J. T. Park and Y.-M. Kang, *Chem. Commun.*, 2011, **47**, 11474-11476.
20 L. Wen, G. Liu, G.-Y. Liu, G.-q. Liu, F. Lia and H.-M. Cheng, *J. Chin. Chem. Soc.,* 2012, **59**,1201-1205.
21 Y. Shiraishi, N. Saito and T. Hirai, *J. Am. Chem. Soc.*, 2005, **127**, 8304–8306.
22 K. K. Mandari, A. K. R. Police, J. Y. Do, M. Kang and C. Byon, *Int. J. Hydrogen Energy*, 2018, **43**, 2073-2082.
23 Y. Liu, R. Xiao, Y. Fang and P. Zhang, *Electrochim. Acta*, 2016, **211**, 1041–1047.
24 C. Qiu, Z. Yuan, L. Liu, S. Cheng, and J. Liu, *Chin. J. Chem.,* 2013, **31**, 819—825.
25 J. Wang, Z. Yang, W. Li, X. Zhong, L. Gu and Y. Yu, *J. Power Sources*, 2014, **266**, 323-331.